南京航空航天大学

论文集

（二〇〇九年） 第5册

航空宇航学院

（第5分册）

南京航空航天大学科技部编

二〇一〇年五月

航空宇航学院

014～015

航空宇航学院2009年学术论文清单（014）

序号	姓名	职称	单位	论文题目	刊物、会议名称	年、卷、期
1	朱程香 朱春玲 付斌	博士 教授 硕士	0141 0141 0141	STUDY ON THE EFFECT OF VISCOSITY AND COMPRESSIBILITY ON ICE ACCRETION	Modern Physics Letters B	2009.23.03
2	姚秋萍 宋保银 赵枚	博士 教授 硕士	014 014 014	Effects of dynamic load on flow and heat transfer of two-phase boiling water in a horizontal pipe	Heat Mass Transfer	2009.45
3	姚秋萍 宋保银 马良军 曹西	博士 教授 硕士 副教授	014 014 014 外单位	Experimental Investigation of Flow Characteristic Air-Water Two-Phase Flow under High Gravity	Transactions of the Japan Society for Aeronautical and Space Sciences	2009.52.175
4	姚秋萍 宋保银 赵枚	博士 教授 硕士	014 014 014	动载下水平管内流动水沸腾两相流型实验研究	中国科技论文在线	2009.021
5	赵枚 宋保银 姚秋萍	硕士 教授 硕士	014 014 014	动载作用下管内汽水两相流传热特性	航空动力学报	2009.24.03
6	毛婷 宋保银 王忠伟	硕士 教授 硕士	014 014 014	沸石5A分子筛吸附乘员舱CO2性能分析	航天医学与医学工程	2009.22.04
7	施红 宋保银 姚秋萍 曹西	硕士 教授 博士 副教授	014 014 014 外单位	Thermal Performance of Stratospheric Airships During Ascent and Descent	Journal of Thermophysics and Heat Transfer	2009.23.04
8	施红 宋保银 姚秋萍	硕士 教授 博士	014 014 014	平流层飞艇太阳能源系统研究	中国空间科学技术	2009.29.01
9	施红 宋保银 周雷 姚秋萍	硕士 教授 研究员 博士	014 014 外单位 014	平流层飞艇的控制模式对其定点特性的影响	航空学报	2009.30.05
10	施红 宋保银 姚秋萍	硕士 教授 博士	014 014 014	平流层飞艇热性能分析软件开发	计算机仿真	2008.25.11
11	单绍荣 宋保银 闫旭东	硕士 教授 硕士	014 014 014	动载和倾斜角度对管内气(汽)液两相流动阻力影响	中国工程热物理学会多相流学术会议	2009年 吉林
12	杨娟 刘卫华	硕士 教授	014 014	地板送风空调系统研究现状与发展	制冷与空调	2009.09.06
13	邓瑾智 刘卫华	硕士 教授	014 014	动力涡轮驱动的逆升压式空气循环制冷系统优化设计	南京航空航天大学学报	2009.41.04
14	方贤德	教授	014	Regression model for thermal performance study of solar heating walls	Proc. of the 4th Canadian Solar Buildings Conferece, Toronto, Canada	
15	方贤德 夏璐璐	教授 硕士	014 014	Heating performance investigation of a bidirectional partition fluid thermal diode	Renewable Energy	2010.35.03
16	方贤德	教授	014	Methodologies for shortening test period of coupled heat-moisture transfer in building envelopes	Applied Thermal Engineering	2009.29.04
17	方贤德	教授	014	直膨式 太阳能辅助热泵技术的研究进展	暖通空调	2009.39.05
18	杨婷婷 方贤德	硕士 教授	014 014	直膨 式太阳能辅助热泵空调热水器及热经济分析	FLUD MACHNERY	2009.37.06
19	张大林 魏涛	教授 博士	014 014	The Numerical Simulation of Flow around Ejection System	Modern Physics Letters B	2009.23.03

20	张大林 陈维建	教授 讲师	014 014	Numerical Investigation of Supercooled Droplets Impingement on Complicated Icing Surface	Modern Physics Letters B	2009.23.03
21	张大林 魏涛 姜南	教授 博士 高工	014 014 外单位	弹射座椅系统外高速流场的数值模拟	南京航空航天大学学报	2009.41.02
22	孟繁鑫 张大林	博士 教授	014 014	微小矩形通道内流动与换热特性	南京航空航天大学学报	2009.41.03
23	魏涛 张大林	博士 教授	014 014	NUMERICAL SIMULATION ON AERODYNAMIC CHARACTERISTICS OF WINDBLAST PROTECTION AT HIGH SPEED	TRANSACTIONS OF NANJING UNIVERSITY OF AERONAUTICS & ASTRONAUTICS	2009.26.04
24	魏涛 张大林	博士 教授	014 014	弹射救生高速气流吹袭防护气动特性数值模拟	应用力学学报	2009.26.04
25	孙建红 许金造	教授 教授	014 外单位	Flow Visualization of Submerged Jets in Narrow Channels	Modern Physics Letters B	2009.23.03
26	孙建红 苏向辉 张翔 周飞	教授 副教授 副教授	014 014 014	民航客机机载蒸发循环系统的关键技术分析	第四届全球華人航空科技研討會	
27	孙建红 颜维旭 李红艳 赵立清	教授 硕士 硕士 博士	014 014 014	民航飞机座舱气相污染物对流扩散数值分析	第四届全球華人航空科技研討會	
28	赵立清 孙建红	博士 教授	014 014	Application of Taylor Series Expansion and Least Squares-based Lattice Boltzmann Method on Simulation of Submerged Plane Water Jets	The sixth International Conference for Mesoscopic Method in Engineering and Science	
29	赵立清 孙建红	博士 教授	014 014	水下平面射流振翅运动数值分析	中国力学学会学术大会2009	
30	赵立清 孙建红 周培培	博士生 教授 学士	014 014 014	Numerical Simulation on Flapping Motion of Submerged Plane Water Jets	Modern Physics Letters B	2009.23.03
31	王从磊 任伟伟 孙建红	博士 硕士 教授	014 014 014	平面圆形伞初始充气阶段的流构耦合研究	中国力学学会学术大会'2009	2009年
32	余莉 史献林 袁文明	副教授 硕士 硕士	014 014 014	牵顶伞在降落伞拉直过程中的作用	南京航空航天大学学报	2009.41.02
33	史献林 余莉 施红	硕士 副教授 硕士	014 014 014	系留气球升空过程的动态模拟	航空学报	2009.30.04
34	李凤志	副教授	014	NUMERICAL SIMULATION FOR EFFECTS OF MICROCAPSULED PHASE CHANGE MATERIAL (MPCM) DISTRIBUTION ON HEAT AND MOISTURE TRANSFER IN POROUS TEXTILES	MODERN PHYSICS LETTERS B	2009.23.03
35	李凤志 李毅 曹业玲	副教授 教授 副教授	014 外单位 副教授	求解织物热湿耦合方程的控制体一时域递归展开算法	南京航空航天大学学报	2009.41.03
36	李凤志 朱云飞 王鹏飞 曹业玲	副教授 硕士 硕士 副教授	014 014 014 014	织物一多种相变微胶囊复合材料热特性数值模拟	南京航空航天大学学报	2009.41.04
37	李凤志	副教授	014	渗流自由面分析的比例边界有限元法	计算物理	2009.26.05
38	苏向辉	副教授	014	STEADY-STATE THERMAL ANALYSIS OF A PLATE FIN HEAT SINK USING GREEN' S FUNCTION SOLUTION	The 3rd International Symposium on Physics of Fluids	

航空宇航学院2009年学术论文清单（015）

序号	姓名	职称	单位	论文题目	刊物、会议名称	年、卷、期
1	余红发 孙伟 张云升 郭丽萍 李美丹	教授 院士 教授 讲师 硕士	015 外单位 外单位 外单位 外单位	Durability of Concrete Subjected to the Combined Actions of Flexural Stress, Freeze-thaw Cycles and Bittern Solutions	*Journal of Wuhan University of Technology-Mater*	2008.23.06
2	余红发 孙伟 麻海燕	教授 院士 讲师	015 外单位 015	混凝土氯离子扩散理论模型的研究I—基于无限大体的非稳态齐次与非齐次扩散问题	南京航空航天大学学报	2009.41.02
3	余红发 孙伟 麻海燕	教授 院士 讲师	015 外单位 015	混凝土氯离子扩散理论模型的研究II—基于有限大体的非稳态齐次与非齐次扩散问题	南京航空航天大学学报	2009.41.03
4	张云清 余红发 王甲春	博士 教授 博士后	015 015 015	SURFACE DAMAGE OF SLAG-CEMENT CONCRETE STRUCTURE EXPOSED TO DEICING-FROST CONDITIONS	International Symposium on Innovation & Sustainability of Structures in Civil Engineering	
5	张云清 余红发 王甲春	博士 教授 博士后	015 015 015	盐冻条件下混凝土结构表面的损伤规律研究	中国公路学报	2009.22.04
6	吴庆令 余红发 王甲春	博士 教授 博士后	015 015 015	Service life and durability of RC structures exposed to Southern and Northern coastal area in China	国际断裂力学FM2009现代力学方法的技术传递与工程应用学术研讨会	
7	吴庆令 余红发 梁丽敏 王甲春 刘连新	博士 教授 博士 博士后 教授	015 015 015 015 外单位	海工混凝土的氯离子扩散性与寿命评估	建筑材料学报	2009. 12. 06
8	吴庆令 余红发 王甲春 梁丽敏	博士 教授 博士后 博士	015 015 015 015	现场海洋区域环境中混凝土的 Cl-扩散特性	河海大学学报(自然科学版)	2009. 37. 04
9	杨礼明 余红发 麻海燕	博士 教授 讲师	015 015 015	Stress corrosion of high performance hybrid fibers reinforced expansive concrete exposed to magnesium sulfate solution	Advanced Materials Research	2009. 79-82
10	杨礼明 余红发 麻海燕	博士 教授 讲师	015 015 015	SULFATE ATTACK IN CONCRETES EXPOSED TO COMBINED ACTION OF FLEXURAL LOAD AND DRY-WET CYCLING	proceedings of the international symposium on innovation & sustainability of structures in civil engineering	2009. 02
11	杨礼明 余红发 麻海燕 周鹏	博士 教授 讲师 硕士	015 015 015 015	Deterioration of high performance hybrid fibers reinforced expansive concrete exposede to magnesium sulfate solution	International conference on transportation engineering 2009	
12	张建业 余红发 麻海燕 燕坤 张伟	硕士 教授 讲师 硕士 硕士	015 015 015 015 015	盐腐蚀与应力作用下混凝土的冻融损伤及抑制	混凝土	2009. 12
13	周　鹏 余红发 杨礼明	硕士 教授 博士	015 015 015	混凝土在氯化镁与硫酸钠复合溶液中的抗腐蚀性	华中科技大学学报	2009. 26. 01
14	吴瑾 黄杰	教授 硕士	土木工程系	低锈蚀率钢筋混凝土梁疲劳性能试验研究	工业建筑	2009.39.42
15	吴瑾 蒋业浩 王浩	教授	15	再生混凝土配合比设计试验研究	低温建筑技术	2009.31.02
16	吴瑾 王浩	教授 硕士	015 015	再生骨料混凝土渗透性试验研究	低温建筑技术	2009.31.05
17	耿殚 吴瑾 赵新铭	博士 教授 副教授	015 015 015	Application of Fiber Bragg Grating Sensor for Rebar Corrosion	2nd International Conference on Smart Materials and Nanotechnology in Engineering, 200 (7)	

序号	姓名	职称	单位	论文题目	刊物、会议名称	年、卷、期
18	耿殚 吴瑾 赵新铭	博士 教授 副教授	015 015 015	Simulation of Fiber Bragg Grating	2nd International Conference on Smart Materials and Nanotechnology in Engineering, 200 (7)	
19	张丹丹 吴瑾 高俊启	硕士 教授 副教授	土木工程系	Investigation and detection on corrosion of concrete structure in marine environment	2nd International Conference on Smart Materials and Nanotechnology in Engineering, 200 (7)	
20	杨桂新 吴瑾 吴文操	博士 教授	015 015	混凝土结构中钢筋腐蚀监测无线传感器	仪器仪表学报	2009.30.06
21	杨曦 吴瑾 梁继光	硕士 教授	015 015 015	再生混凝土抗拉强度与抗压强度关系的试验研究	四川建筑科学研究	2009.35.05
22	张英杰 吴瑾	硕士 教授	015 015	混凝土裂缝自修复技术试验研究	低温建筑技术	2009.31.10
23	陆耀清 艾军 徐春林 钱江	硕士 教授 硕士 硕士	015 015 015 015	预应力CFRP布加固RC梁固有频率的试验	汶川地震后工程结构安全与防灾新进展/江苏省土木工程结构安全与防灾学术交流会	2009年12月
24	李厚海 艾军 潘建伍 钱江	硕士 教授 讲师 硕士	015 015 015 015	基于摩擦-胶接机理的混合锚固技术的有限元分析	汶川地震后工程结构安全与防灾新进展/江苏省土木工程结构安全与防灾学术交流会	2009年12月
25	徐春林 艾军 杨杰	硕士 教授 讲师	015 015 015	船舶撞击桥梁理论计算模型的初探	汶川地震后工程结构安全与防灾新进展/江苏省土木工程结构安全与防灾学术交流会	2009年12月
26	陈少林 李燕秀	副教授 硕士	015 015	一种高效的局部径向基点插值无网格方法	固体力学学报	2009.30.01
27	陈少林 唐敢 刘启方 丁海平	副教授 副教授	015 015 外单位 外单位	三维土-结构力学相互作用的一种时域直接分析方法	防震减灾工程理论与实践新进展	
28	张毅 陈少林	硕士 副教授	015 015	基础阻抗函数的时域求解方法	防震减灾工程理论与实践新进展	
29	高培伟	教授	一院	Study on Novel Repair Materials and Techniques for Airport Pavement	International Conference on Transportation Engineering	2007, July 22-24
30	**高培伟** **耿飞** **卢小林**	教授 讲师	015 015	Hydration and expansion properties of novel concrete expansive agent	Key Engineering Materials	2009, 405-406: 267-271
31	**高培伟** **卢小琳** ?	教授 讲师	015 015	Shrinkage and expansive strain of concrete with fly ash and expansive agent	Journal of Wuhan University of Technology Materials Science	2009.24
32	石南南 陈波 张辉 高培伟	硕士 硕士 教授	015 015 015	大坝混凝土温度应力数值模拟	低温建筑技术	2009.02
33	张辉 丁建彤 高培伟	硕士 教授	015 外单位 015	混凝土气孔结构自动测试方法对比分析	**低温建筑技术**	2009, 138(12): 7-10
34	张辉 高培伟 石南南	硕士 教授 硕士	015 015 015	混凝土气泡特征参数测试方法研究	红水河	2009.28.04
35	高俊启 陈昊 季天剑 刘宏月	副教授 硕士 副教授 硕士	015 015 015 015	沥青路面动水压力光纤传感测量研究	传感器与系统	2009.28.09

序号	姓名	职称	单位	论文题目	刊物、会议名称	年、卷、期
36	高俊启 季天剑	副教授 副教授	015 015	橡胶沥青应力吸收层力学与疲劳性能研究	实验力学	2009.24.04
37	解建光 张雪 李贺	副教授	015 外单位 外单位	高速公路路面雨水径流有机污染物赋存状态研究	中国环境科学	2009.29.10
38	李俊 吴瑾 高俊启	讲师 教授 副教授	015 015 015	混凝土结构光纤光栅腐蚀传感器	中国腐蚀与防护学报	2009.29.02
39	季斌 麻海燕 余红发 程宇	博士 讲师 教授 硕士	015 015 015 015	三维编织钢纤维增强渍浆混凝土的受压力学性能	南京航空航天大学学报	2009.41.05
40	胡蝶 麻海燕 余红发 曹文涛 翁智财	硕士 讲师 教授 硕士 硕士	015 015 015 015 015	矿物掺合料对混凝土氯离子结合能力的影响（英文）	硅酸盐学报	2009.37.01
41	刘俊龙 麻海燕 王甲春	硕士 讲师 博士后	015 015 015	干燥环境条件下大掺量矿物掺合料高强混凝土的抗冻性	混凝土	2009.02
42	唐敢 陈少林 王法武 丁海平	副教授 副教授 讲师 教授	015 015 015 外单位	空间结构-地基动力相互作用的三维时域数值分析方法	工程力学	2009.26.08
43	唐敢 朱奕锋 曾滨	副教授	015 外单位 外单位	吉林速滑馆悬索钢结构屋盖稳定及抗震性能分析	应用力学学报	2009.26.03
44	王法武	讲师	15	TOTAL AND INCREMENTAL ITERATION FORCE RECOVERY PROCEDURE FOR THE NONLINEAR ANALYSIS OF FRAMED STRUCTURES	ADVANCED STEEL CONSTRUCTION	2009.05.04
45	王喆	副教授	15	Energy evaluation of inelastic structures subjected to random earthquake excitations	THE STRUCTURAL DESIGN OF TALL AND SPECIAL BUILDINGS	2009.18.05
46	张丽芳 艾军	讲师 教授	015 015	Method for Bridge Bearing Capacity Assessment Based on Analytic Hierarchy Process	南京航空航天大学学报（南京航空航天学）	2009.03.26
47	张丽芳 艾军	讲师 教授	015 015	桥头引道沉降对简支梁冲击效应的影响力	振动与冲击	2009.28.10

Modern Physics Letters B, Vol. 23, No. 3 (2009) 481–484

World Scientific
www.worldscientific.com

STUDY ON THE EFFECT OF VISCOSITY AND COMPRESSIBILITY ON ICE ACCRETION

ZHU CHENGXIANG

College of Aerospace Engineering, Nanjing University of Aeronautics and Astronautics, 29 Yudao Street, Nanjing 210016, China
zcx2007@nuaa.edu.cn

ZHU CHUNLING

College of Aerospace Engineering, Nanjing University of Aeronautics and Astronautics 29 Yudao Street, Nanjing 210016, China
clzhu@nuaa.edu.cn

FU BIN

College of Aerospace Engineering,Nanjing University of Aeronautics and Astronautics 29 Yudao Street, Nanjing 210016, China

Received 1 June 2008

Ice accretion on aircraft is studied by a numerical method. By solving governing equations, the flow field is obtained for analyzing the icing zone and calculating the ice quantity on different parts. Influence of the fluid viscosity and compressibility on icing characters is extensively studied. And it can be found that the results agree well with those calculated by LEWICE program. This achievement could be helpful to further research on ice accretion.

Keywords: Icing; Fluid field; viscosity; compressibility.

1. Introduction

Icing on aircraft can bring many problems, thus icing accretion needs be studied for selecting suitable anti-icing or de-icing system.

Finite volume method can be used to solve both Euler equations and Navier-Stokes (N-S) equations. As a result, inviscid and viscous flow fields can be obtained respectively. The obtained results can then be used to determine the droplet trajectories and ice shapes.

2. Droplet Trajectory Analysis

Lagrangian approach is used to calculate water droplet trajectories. According to the Newton's Second Law, for a single droplet, differential equations are established based on the following assumptions[2]:

- As the liquid water content (LWC) rarely exceeds 2.0 g/m^3, the influence of the droplet on the flow field is neglected.
- Gravitation is neglected and the droplet remains spherical with fixed diameter, and has no phase transformation since its size is so small ($10 \le d \le 50\ \mu$m).
- As the density of water is much greater than that of air, the pressure gradient term, the apparent mass term, and the Bassett unsteady memory term are negligible.
- Temperature, viscosity and density of the droplet remain the same at any time.

Thus the equations of motion for the droplets can be written as follows:

$$\frac{d\vec{u}}{d\tau} = \frac{C_D \operatorname{Re} w}{24} \cdot \frac{1}{K} \cdot (\vec{v} - \vec{u}) \tag{1}$$

where, $\vec{u}, \vec{v}$ are the speed of water and air respectively. C_D is coefficient of the drag force. Reynolds number of water is $\operatorname{Re} w$, and K is coefficient of inertia.

3. Ice Accretion Analysis

To simulate ice accretion, a control volume[3] is used, whose upper limit is the boundary layer and lower limit is the ice surface. As any control volume coincides with the rules of mass and energy conservation, the following equations can be obtained.

$$\dot{m}_c + \dot{m}_{rin} - \dot{m}_e - \dot{m}_{rout} = \dot{m}_i \tag{2}$$

$$\dot{m}_c i_{w,T} + \dot{m}_{rin} i_{w,sur(i-1)} = \dot{m}_e i_{v,sur} + \dot{m}_{rout} i_{w,sur} + \dot{m}_i i_{i,sur} + q_a \Delta s + q_k \Delta s \tag{3}$$

where $\dot{m}_c$ is the mass flow rate of collected water droplets and $i_{w,T}$ is the corresponding enthalpy. $\dot{m}_{rin}$ is the mass flow rate which enters the control volume from upstream control volume and $i_{w,sur(i-1)}$ is the corresponding enthalpy. $\dot{m}_e$ is the evaporative mass flow rate and $i_{v,sur}$ is the corresponding enthalpy. $\dot{m}_{rout}$ is the mass flow rate of liquid water out of the control volume and $i_{w,sur}$ is the corresponding enthalpy. $\dot{m}_i$ is the ratio of the amount of water freezing and $i_{i,sur}$ is the corresponding enthalpy. q_a is the convective heat transfer rate and q_k is the conductive heat transfer rate.

4. Comparison

Under conditions of Table 1, a series of water droplet trajectories of NACA0012 and ice shapes on its surface are studied.

Table 1. Conditions of calculation.

Attack angle	Flight speed	Flight altitude	LWC	MVD	Accretion time
0^0	129 m/s	900 m	0.5 g/m^3	20 μm	60 s

Using finite volume method to solve Euler equations, inviscid and incompressible flow field can be obtained. The results are used to solve equation (2), and water droplet trajectories without considering viscosity and compressibility can be obtained, as shown

in Figure 1 (left one). On this basis, equation (3) can be solved and ice shapes can be obtained, as shown in Figure 2 (left one). Similarly, N-S equations are solved by using finite volume method for obtaining viscous and compressible flow field. And then results are used to solve equations (2) and (3) orderly to determine the water droplet trajectories and ice shapes, as shown in Figure 1 (right one) and Figure 2 (middle one). LEWICE uses Douglas two-dimensional potential flow program to solve the flow field with considering viscosity and compressibility, and uses its own program to obtain the ice shapes, as shown in Figure 2 (right one).

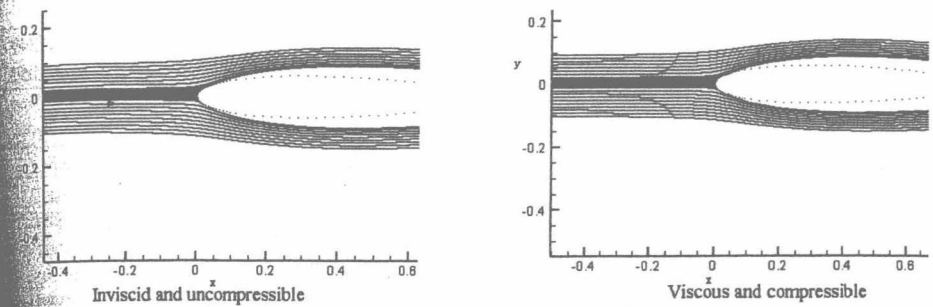

Figure 1 Comparison of droplet trajectories

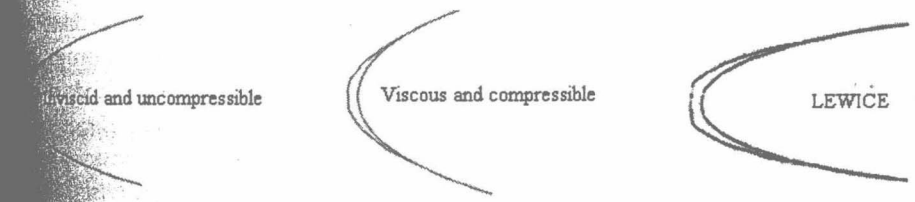

Figure 2 Comparison of ice shapes

ng the two drawings in Figure 1, differences cannot clearly been shown, because are too dense. Thus some data are listed in Table 2, from which it can be learned istance error of the points impacting on the wing surface for the same Y0 is

Table 2. Data associated with Figure 1.

Coordinates	Y0 = –0.01	Y0.= –0.0022	Y0 = 0.0098
Xend	0.0082	0.0042	0.007799
Yend	–0.0158	–0.00314	0.154318
Xend	0.0075	0.0022	0.00717
Yend	–0.0142	–0.00318	0.1477
	0.001746	0.002	0.0066

ginal vertical coordinate of the water droplet trajectory. Xend and Yend is the horizontal and of the water droplet trajectory which impacts on the wing surface, respectively.

clearly shown that the ice shapes both with considering viscosity and and without consideration have the same tendency as that of the LEWICE

program. This indicates that methods used in this paper are correct. Furthermore, the ice shape with considering viscosity and compressibility is more close to the result of LEWICE program, and there is much difference between the ice shapes in inviscid and incompressible flow field and those in viscous and compressible flow field. The specific data are listed in Table 3. It clearly shows that the relative error of ice thickness has exceeded 30%. Thus, in the conditions studied in this paper, viscosity and compressibility cannot be neglected.

Table 3. Relative error of ice thickness.

		Xend = 2.0935 Yend = –0.058	Xend = 0.000419 Yend = –0.00314	Xend = 0.249 Yend = 0.059
Ice thickness (mm)	Inviscid and uncompressible	1.236	1.793	1.322
	Viscous and compressible	2.05	4.885	2.50
Distance error		39%	58%	47%

5. Conclusions

Finite volume method can be used to solve both Euler equations and N-S equations. In this way, inviscid and viscous flow fields can be obtained respectively. The results can be used to determine water droplet trajectories and ice shapes. Two groups of data were obtained. Comparing these two groups of results with those of the LEWICE program, it can be found that the ice accretion tendency of the three is similar, so the methods used in this paper is thought to be right. Actually, the ice shape with considering viscosity and compressibility is closer to that of the LEWICE program, and the relative error of the ice thickness is more than 30%. So, in the conditions presented in this paper, viscosity and compressibility should be considered.

As there are many assumptions, the ice scale calculated in this paper does not agree with that of LEWICE program very well. In future studies, more effort will be made to take the effect of viscosity and compressibility into account in the study of ice accretion.

References

1. S. Thomas and R. Cassoni, Aircraft Anti-Icing and Deicing Techniques and Modeling, 34th Aerospace Sciences Meeting & Exhibit, AIAA 96-09390 (1996).
2. E.P. Schuster, J.M. Gambill, M.S. Fisher, Computational Icing Analysis of Aircraft inlets, AIAA/SAE/ASME/ASEE 28th Joint Propulsion Conference and Exhibit, AIAA 92-3178
3. Keiko Yamaguchi and R. John Hansman Jr, Heat Transfer on Accreting Ice Surfaces, Massachusetts Institute of Technology, Cambridge, Massachusetts 02139, Vol. 29. No. 1.
4. G. Mingione, V. Brandi, B. Esposito, Ice Accretion Prediction on Multi-Element Airfoils, American Institute of Aeronautics and Astronautics, 1997.
5. Abdelkader Baggag, Mondher Chekki and Wagdi G. Habashi, Parallelization of a finite volume scheme applied to ice accretion. 36th AIAA Fluid Dynamics Conference and Exhibit, 2006.

Heat Mass Transfer (2009) 45:1205–1213
DOI 10.1007/s00231-009-0496-7

ORIGINAL

Effects of dynamic load on flow and heat transfer of two-phase boiling water in a horizontal pipe

Qiu-ping Yao · Bao-yin Song · Mei Zhao · Xi Cao

Received: 14 April 2008 / Accepted: 4 May 2009 / Published online: 23 May 2009

Abstract An experimental investigation was performed to obtain the flow and heat transfer characteristics of single-phase water flow and two-phase pipe boiling water flow under high gravity (Hi-G) in present work. The experiments were conducted on a rotating platform, and boiling two-phase flow state was obtained by means of electric heating. The data were collected specifically in the test section, which was a lucite pipe with inner diameter of 20 mm and length of 400 mm. By changing the parameters, such as rotation speed, inlet temperature, flow rate, and etc., and analyzing the fluid resistance, effective heat and heat transfer coefficient of the experimental data, the effects of dynamic load on the flow and heat transfer characteristics of single phase water and two-phase boiling water flow were investigated and obtained. The two-phase flow patterns under Hi-G condition were obtained with a video camera. The results show that the dynamic load significantly influences the flow characteristic and boiling heat transfer of the two-phase pipe flow. As the direction of the dynamic load and the flow direction are opposite, the greater the dynamic load, the higher the outlet pressure and the flow resistance, and the lower the flow rate, the void fraction, the wall inner surface temperature and the heat transfer capability. Therefore, the dynamic load will block the fluid flow, enhance heat dissipation toward the ambient environment and reduce the heat transfer to the two-phase boiling flow.

Q. Yao (✉) · B. Song · M. Zhao
Department of Man-Machine-Environment Engineering,
Nanjing University of Aeronautics and Astronautics,
210016 Nanjing, People's Republic of China
e-mail: yiaoqiuping@163.com

X. Cao
Faculty of Engineering, Shinshu University,
Nagano 3808553, Japan

1 Introduction

Boiling heat transfer coupled with gas-liquid two-phase flow is a thermal process,which is accompanied by phase change. The two-phase flow and boiling heat transfer in a horizontal pipe is widely used in power, nuclear energy, chemistry, aerospace, refrigeration, air-conditioning and other industry processes. When the vapor cycle cooling system is boarded on a vehicle, it must be suffered from the dynamic load during an accelerating, decelerating or maneuver flight. The dynamic load will certainly influence condensation, evaporation, flow and heat transfer of refrigerant in airborne vapor cycle cooling system, and therefore the performance of refrigeration components and system. The reliability of the vapor cycle cooling system is very important for its use in flight vehicles and the better understanding of the flow and heat transfer fundamentals of the gas–liquid two-phase fluid under high gravity will increase its safety during its operation in flight.

In recent years, the researchers in two-phase flow field have focused on the characteristics of two-phase flow under microscale [2, 10, 16, 21], microgravity [9, 14, 17, 19] and rotation [1, 4–6, 12, 13, 15, 18] conditions. There were few reports in the flow and heat transfer mechanism of two-phase fluid under Hi-G condition, which is normally encountered in maneuver flight. For the aircraft engine turbine blade and the airborne vapor cycle cooling system, the effects of Hi-G condition on two-phase flow and boiling heat transfer are greatly needed to be investigated. The phase change or boiling will cause mass transfer and the

change of void fraction. Not only would the flow patterns change along the flow channel, but also with magnitude of dynamic load. All these lead to the complication of flow computation, and make the continuity, momentum, energy equations more complicated. Therefore, two-phase flow with boiling under Hi-G condition is one of the complicated two-phase flow phenomena which have more influence factors. It is better to begin the investigation from an empirical approach. An experimental research on the effects of Hi-G condition on the flow and heat transfer characteristics of two-phase boiling water flow in a horizontal pipe has been conducted in this paper.

2 Experimental apparatus

A rotational platform was designed in the experiment to simulate the Hi-G condition. Experimental system of steam-water two-phase flow with Hi-G condition includes a closed water cycling pipeline loop, a rotational platform, a heating system, a test section, a data measuring and recording system and a video camera. The experimental system is shown in Fig. 1. The test section is a lucite pipe which is installed in radius. The solid line in Fig. 1 denotes the experimental pipeline, and the dash line denotes the signal transmission line.

During the experiment, the water drawn from the water tank by water pump goes through a pre-heater first, then flows into the transparent test section, where it is heated again to boiling two-phase flow by a resistance wire heater, and finally returns to the water tank. After the gas is drained, the water is waiting for repumping. The transparent test section is a lucite pipe with inner diameter of 20 mm and length of 400 mm. It is divided into two parts. The first half part is a heating zone. There are 3 cross-sections for temperature measurement and each of them installs 3 thermocouples, as shown in Fig. 1. They are used to measure the mainstream temperature of the fluid and the inner-wall temperatures directly. The second-half part is photographing area. At the middle of the test section, a circular electric-conduct probe is installed for measuring the void fraction of the fluid. With the pressure transducer, pressure gauge, electric-conduct probe and thermocouples, the pressure drop, outlet pressure, void fraction, as well as the inlet and outlet fluid temperatures of heating section and inside-wall temperatures are measured in the test section. The electrical signals of these data are transmitted to acquisition module of ADAM-4017 and 4018, and then to the computer through ADAM-4520. Using the VB program, the real-time data acquisition is realized. The ambient room temperature is read directly from a thermohygrometer. The rotational speed of the platform is adjusted by regulating the resistance of frequency converter to achieve different dynamic loads.

The visible system is used to observe and record the change of boiling two-phase flow patterns under Hi-G condition. In the experiment, the two-phase flow pattern transition is recorded with a video camera, which is installed in front of the test pipe and rotated with the test section synchronously. A non-reflection background screen is installed behind the test section. The lighting is supplied by a 105 W energy saving tricolor lamp.

3 Results and discussion

3.1 Effect of dynamic load on boiling two-phase flow pattern in horizontal pipe

The two-phase flow pattern is extremely unstable, and there are different flow pattern transitions under different heating

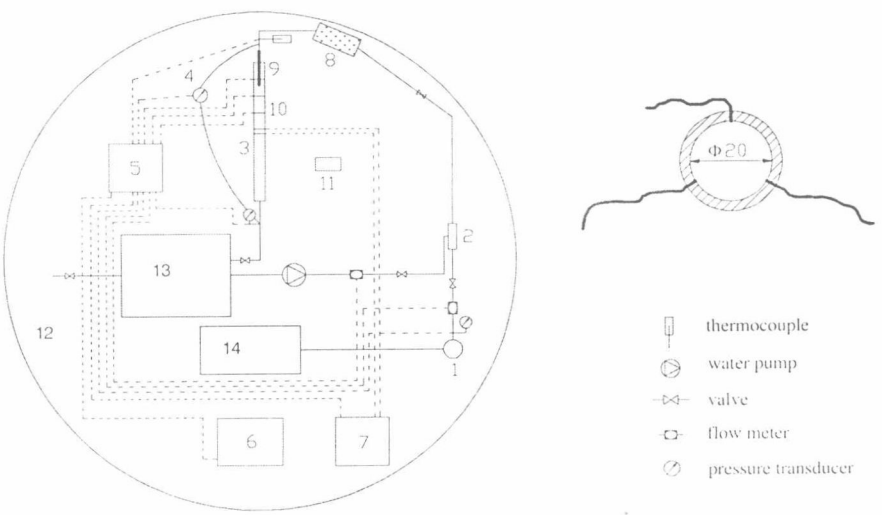

Fig. 1 Schematic diagram of experimental apparatus. 1 regulator; 2 mixer; 3 transparent test pipe(circular probe inside); 4 pressure drop transducer; 5 data acquisition module; 6 note-computer; 7 void fraction identifying instrument; 8 pre-heater; 9 resistance wire heater; 10 thermocouple; 11 video camera; 12 rotating platform; 13 water tank; 14 air compressor (for other use)

and flowing conditions. Two-phase flow patterns under Hi-G condition can also appear the unique characteristic. The instabilities of two-phase flow pattern as well as the forces acting on fluid will lead to the transition between flow patterns. In general, the phenomenon of resistance [8, 11] can be used to explain the transition between slug flow and churn flow, and the phenomenon of reverse [3] can be used to explain the transition between churn flow and annular flow. In the experiment, there is two-phase wavy flow in the pipe under the heating condition with constant heat flux. The transition of two-phase flow pattern under Hi-G is quite different from that under normal gravity, i.e. stationary state. When the platform rotation speed increases gradually, there are no typical slug flow and churn flow in the test pipe, but the impact phenomenon between two phases. Therefore the impact phenomenon will be used to explain the transition between wavy flow and plug flow.

The images of two-phase pipe flow of boiling water heated at constant heat flux under different platform rotation speeds and flow rates were shot and recorded with a video camera. The boiling two-phase flow pattern photos intercepted from the image shot in the period of increasing the dynamic load from 0 to 2G (means 2 times of terrestrial gravity) are shown in Fig. 2. Figure 2a shows wavy stratified flow pattern in the static state, in which the dynamic load G_x is 0, and liquid-phase flow rate is 0.1728 m^3/h. The phase interface can be seen clearly. When turning on the frequency modulator to rotate the rotating platform, there is a small centrifugal force or dynamic load exerting on the fluid. As the dynamic load reaches the value of 0.21G, centrifugal force and inertial force affect the gas-phase and liquid-phase respectively, and the shock-wave appears in the gas-liquid interface. The distribution of steam and water can be seen clearly. This flow pattern is defined as impact flow, as shown in Fig. 2b. When dynamic load reaches the value of 0.95G, the influence of centrifugal force on two-phase flow is greater, and the impact phenomenon is even more severe. The extrusion on steam-water interface is so severe that the steam and water are mixed together and there is no continuous interface between them. This flow pattern is defined as intense impact mixing flow, as shown in Fig. 2c. When the rotation speed continues to increase, the fluid pressures increase further. As the dynamic load reaches the value of 1.23G, the steam decreases significantly and the impact between two phases becomes weaker. The water phase plays a dominant role. This flow pattern is defined as impact mixing flow, as shown in Fig. 2d. When the rotation

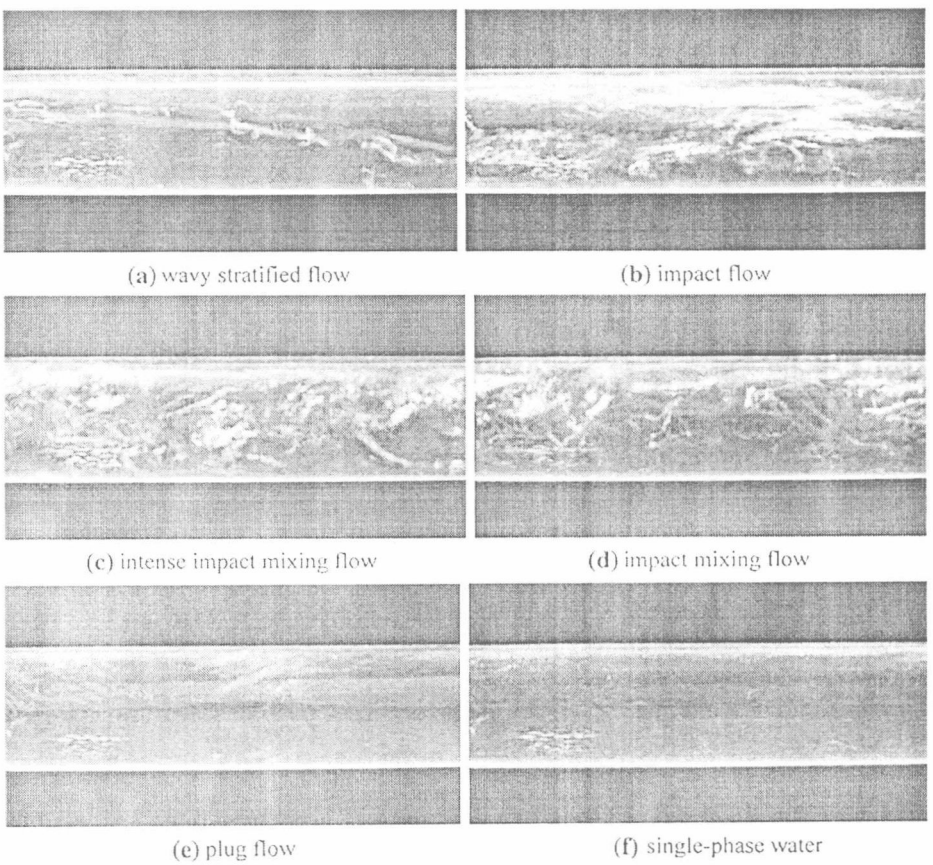

Fig. 2 Steam-water two-phase flow pattern photos during increasing dynamic load

speed increases further, the dynamic load is increased further. The increased heat loss and liquid pressure make the transition from boiling two-phase flow to single-phase water flow gradually. When the dynamic load reaches the value of 1.58G, the flow pattern becomes plug flow, and the droplets are contained in the bubbles, which is similar to the static state. But there is no obvious gas-liquid interface between bubble and water, as shown in Fig. 2e. As the dynamic load reaches the value of 2G, the fluid in pipe becomes single-phase water flow, as shown in Fig. 2f. The momentum equation for phase k could be expressed as [20]:

$$\frac{\partial}{\partial t}(\rho_k \alpha_k u_k) + \frac{1}{A}\frac{\partial}{\partial z}(\rho_k \alpha_k A u_k^2) + \frac{1}{A}\frac{\partial}{\partial z}(\alpha_k A p_k) + \rho_k \alpha_k \vec{a}_k - \frac{C_k^W}{A}\tau_k^W = M_k^i \quad (1)$$

where α_k is the volume fraction of phase k; C_k^W is the friction perimeter, m; τ_k^W is the wall shear stress, N/m^2; $\vec{a}_k$ is the total acceleration, m/s^2; and M_k^i is the momentum transferred through the gas–liquid interface, N/m^3. From the equation, we can see that the two-phase flow characteristic in the present work is affected by the phase change, and the body forces including gravity, dynamic load and Coriolis force, besides the common parameters such as pressure, shear stress and inertial force. On the action of the above forces, the two phases impact each other intensively. The increased pressure and heat loss with increasing rotational speed finally lead the steam-water two-phase flow to single-phase water flow.

3.2 Flow and heat transfer characteristics of steam-water two-phase flow in horizontal pipe under Hi-G condition

A series of experiments on single-phase water flow and its boiling heat transfer in a horizontal smooth pipe were performed and a great amount of experimental data was obtained. The parameter ranges are 0.1–0.25 m^3/h for flow rate, 95 kW/m^2 for heat flux, 10–97°C for inlet temperature, 0–100% for void fraction and 0–2G for dynamic load or gravity.

The flow and heat transfer characteristics of single-phase water and steam-water two-phase flow under Hi-G condition were given and analyzed as follows.

3.2.1 Heat transfer characteristic of single-phase water pipe flow under Hi-G condition

In the experiment fluid flows in radial pipe, and the fluid medium is single-phase water heated continuously with two electrical heaters. The direction of gravitational acceleration under Hi-G condition is the same as the fluid flow direction. After adjusting the experimental state to steady state at static, the frequency modulator is turned on and the platform is rotated. When angular speed is increased to 57 r/min, i.e. the dynamic load reaches the value of 2G, the speed gradually drops to zero. Figure 3 presents the history of outlet pressure P_2, pressure drop ΔP, flow rate Q, and inlet temperature T_{in} in test pipe under Hi-G condition. With the rotation speed changing, these parameters change

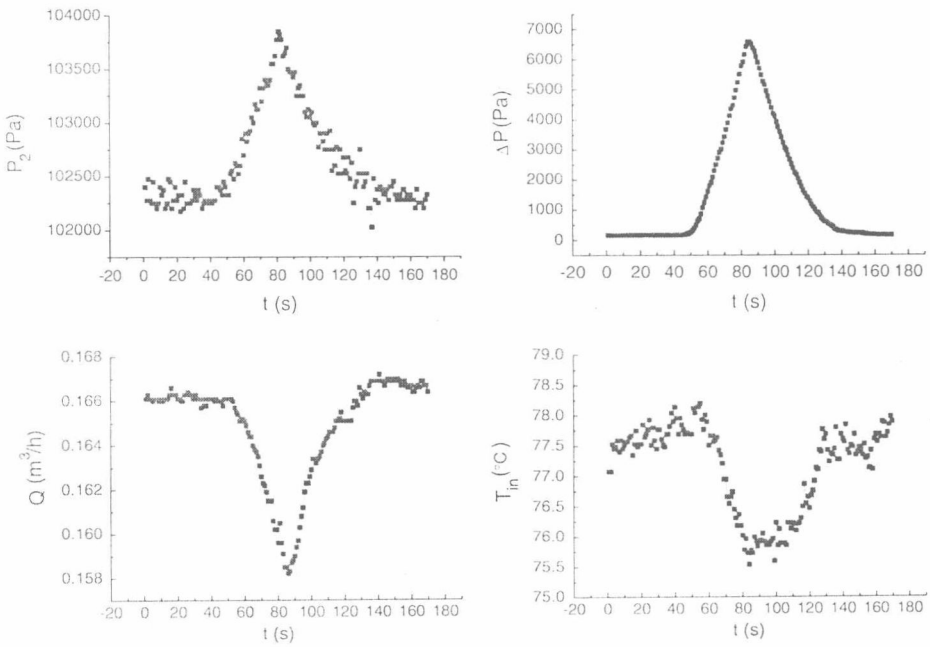

Fig. 3 History of single-phase hot water flow parameters under Hi-G condition

continuously. As shown in Fig. 3, as the rotation speed increases, the outlet pressure and pressure drop increase, but the flow rate and inlet temperature reduce. On the contrary, as the rotation speed reduces, the outlet pressure and pressure drop decrease, but the flow rate as well as inlet temperature increase. When the dynamic load reaches 2G, the flow parameters arrive to their limiting values. The change of each flow parameter during acceleration and deceleration is about symmetrical around the limiting value. After the rotating platform is stopped, all parameters almost return to the same values at the static state.

The period in 0–50 and 120–170 s is for static state responding to the platform before and after rotation, respectively. As shown in Fig. 3, as the result of continuous heating, the fluid temperature rises slowly over the time period. The reason for the fluid parameter changing with dynamic load is analyzed as follows. The rotation causes the dynamic load to be exerted on the fluid with an inverse direction. The flow resistance, and therefore the pressure and pressure drop in the test section are increased so that the flow rate decreases. With the increase in rotation speed, the convective heat transfer outside test pipe is enhanced. The total heat dissipation of the inside fluid increases, which decreases the fluid temperature. When rotation speed reduces, the heat dissipation decreases, and the fluid temperature rises again. When the rotation speed reduces to zero, the radiation becomes the main way in heat dissipation, and the fluid temperature returns to the value before rotation.

After processing the experimental data, the variations of flow and heat transfer parameters of single-phase water with dynamic load were obtained for inlet temperatures of 65 and 83°C, respectively. Figure 4 presents the variations of flow parameters of single-phase water with dynamic load. As the dynamic load increases, the water flow rate and Reynolds number decrease, and the pressure drop and outlet pressure increase. Though the variation rates of flow rate and Reynolds number with the dynamic load for 65°C water and 83°C water are different, the variations of the pressure drop or outlet pressure with dynamic load are almost the same. It is evidenced that the effects of flow rate and inlet temperature on the pressure drop are far less than that of dynamic load. Initial flow rate is controlled to get different initial inlet temperature. Re_l is the flow Reynolds number in the pipe of 10 mm inner diameter, which is connected with the entrance of the transparent test section. It is defined as:

$$Re_l = ud_m/\nu_l \tag{2}$$

where u is the velocity of single-phase liquid, m/s; $d_m = 10$ mm is the inner diameter of inlet heat section; and ν_l is the liquid kinematic viscosity, m^2/s. Based on the value of Re_l, the flow in the test pipe keeps turbulent flow during the experimental process.

The reason for the variation mentioned above could be explained as follows. Figure 5 presents schematic diagram of fluid flow and load. The radial test section is installed on the platform and the fluid in it flows from point A to point B.

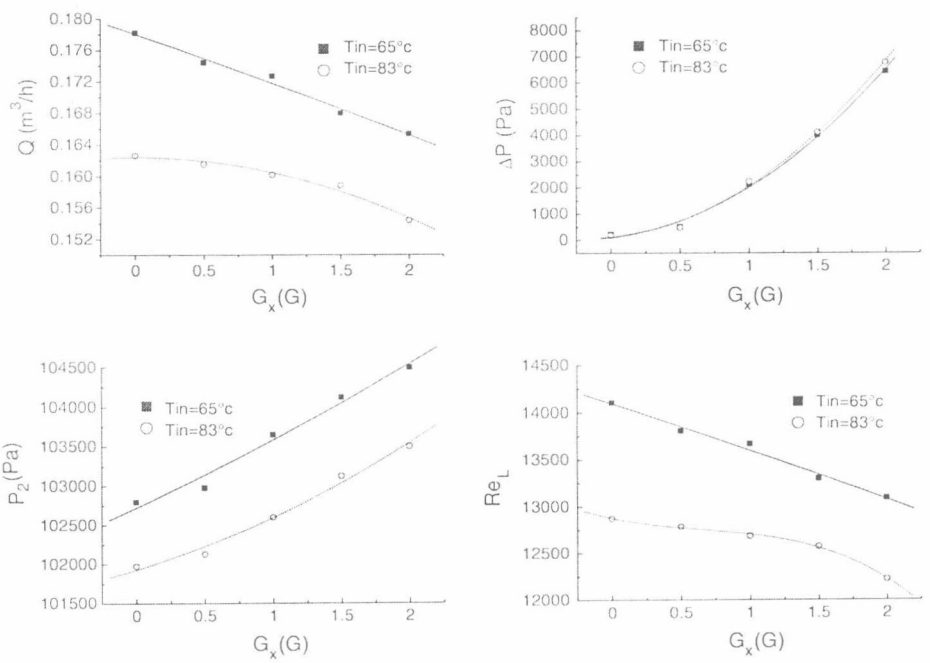

Fig. 4 Variation of single-phase water flow parameters with dynamic load

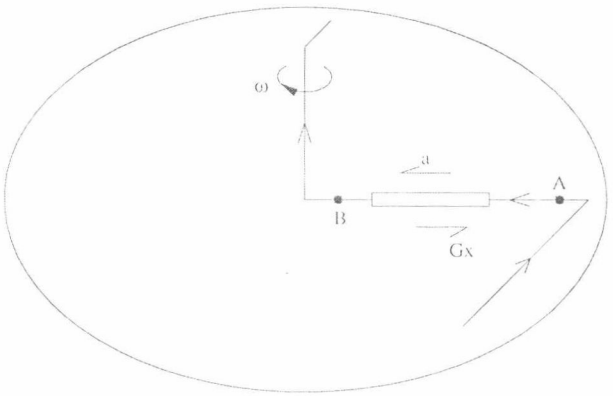

Fig. 5 Schematic of fluid flow and load

That is, the fluid flow direction is in radial direction toward the platform center and the platform rotates clockwise around its circular center. The fluid flow direction in the test section is opposite to that of the centrifugal force or the dynamic load G_x generated by rotation, which will be exerted on the fluid and blocks its flow. The greater the dynamic load, the more obvious the tendency. In a uniform rotation with a certain rotation speed, the absolute value of the acceleration, whose direction is toward center, is proportional to the distance from center. That is the value increases from B to A. The direction of centrifugal force or the dynamic load is opposite to the flow direction, which causes the pressure drop and inlet pressure increase, and the flow rate decreases. The bigger the value, the bigger the flow resistance. The present experimental data agree with the experimental ones by Ma [7] and the numerical results simulated by Liu [5].

Figure 6 shows the variations of heat transfer parameters with dynamic load, which is gotten from the processed data originally presented in Fig. 4. Effective heat reflects the heat transfer to the fluid in the pipe. As shown in Fig. 6, whatever the inlet temperature is 65 or 83°, effective heat will decrease with the increase in dynamic load, which is mainly due to the rotation enhanced heat losing. The higher fluid temperature can also enhance heat dissipation. Therefore the fluid effective heat for inlet temperature of 83° is lower than that for inlet temperature of 65°. ΔT is the temperature difference between mainstream fluid and the wall inner surface, and it is defined as $(T_{in} + T_{out})/2 - T_{w1}$, which increases with dynamic load. As the dynamic load increases from 0.5 to 1.5 G, the increased magnitude of temperature difference is small, but the temperature difference for inlet temperature of 65° is higher than that of 83°. As the dynamic load exceeds 1.5 G, the temperature difference increases rapidly due to enhanced heat dissipation. h is external heat transfer coefficient of internal fluid, which can be expressed as:

$$h = \frac{q_{loss}}{A(T_f - T_{w1})} = \frac{q_{loss}}{A[(T_{in} + T_{out})/2 - T_{w1}]} \tag{3}$$

where $q_{loss} = P - q_e$, is the difference between the total heating power P and the effective heat q_e. As the dynamic load changes from 0 to 1.5 G, h increases with dynamic load. As the dynamic load exceeds 1.5 G, the rapidly

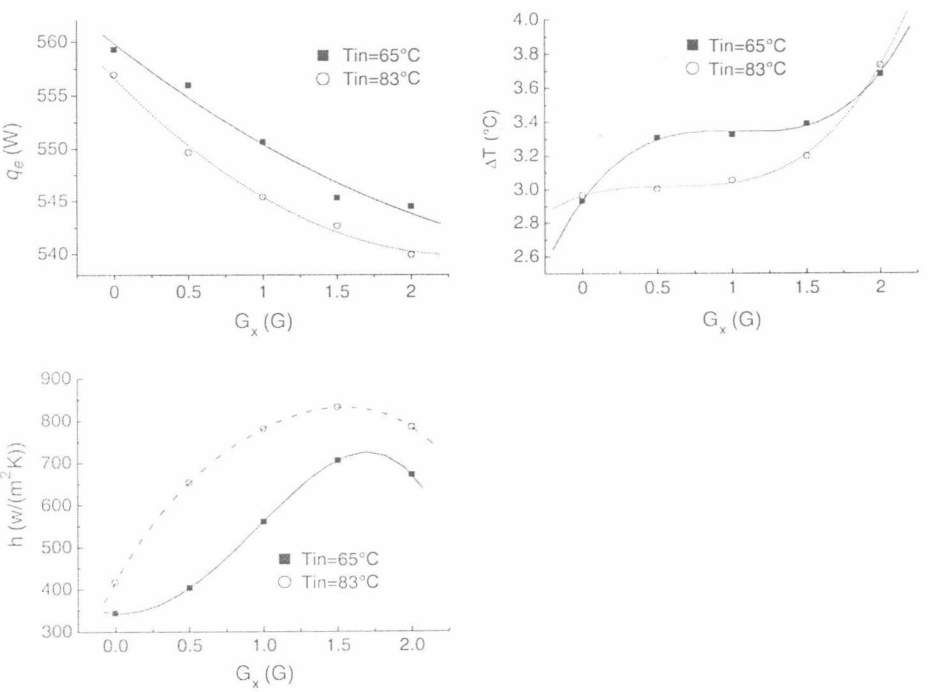

Fig. 6 Variation of single-phase hot water heat transfer parameters with dynamic load